**Atmospheric
Chemistry
and Physics**

The Hohenpeissenberg aerosol formation experiment (HAFEX): a long-term study including size-resolved aerosol, H_2SO_4, OH, and monoterpenes measurements

W. Birmili[1], H. Berresheim[2], C. Plass-Dülmer[2], T. Elste[2], S. Gilge[2], A. Wiedensohler[3], and U. Uhrner[3]

[1]University of Birmingham, Division of Environmental Health and Risk Management, Birmingham, B15 2TT, UK
[2]German Weather Service, Meteorological Observatory Hohenpeissenberg (MOHp), Albin-Schwaiger-Weg 10, 83282 Hohenpeissenberg, Germany
[3]Institute for Tropospheric Research, Permoserstrasse 15, 04303 Leipzig, Germany

Abstract. Ambient aerosol size distributions (> 3 nm) and OH, H_2SO_4, and terpene concentrations were measured from April 1998 to August 2000 at a rural continental site in southern Germany. New particle formation (NPF) events were detected on 18% of all days, typically during mid-day hours under sunny and dry conditions. The number of newly formed particles correlated significantly with solar irradiance and ambient levels of H_2SO_4. A pronounced anti-correlatation of NPF events with the pre-existing particle surface area was identified in the cold season, often associated with the advection of dry and relatively clean air masses from southerly directions (Alps). Estimates of the particle formation rate based on observations were around $1\,cm^{-3}\,s^{-1}$, being in agreement with the predictions of ternary homogeneous H_2SO_4-NH_3-H_2O nucleation within a few orders of magnitude. The experimentally determined nucleation mode particle growth rates were on average $2.6\,nm\,h^{-1}$, with a fraction of $0.7\,nm\,h^{-1}$ being attributed to the co-condensation of H_2SO_4-H_2O-NH_3. The magnitude of nucleation mode particle growth was neither significantly correlated to H_2SO_4, nor to the observed particle formation rate. Turn-over rate calculations of measured monoterpenes and aromatic hydrocarbons suggest that especially the oxidation products of monoterpenes have the capacity to contribute to the growth of nucleation mode particles. Although a large number of precursor gases, aerosol and meteorological parameters were measured, the ultimate key factors controlling the occurence of NPF events could not be identified.

Correspondence to: W. Birmili (w.birmili@bham.ac.uk)

1 Introduction

Atmospheric particulates contribute to light scattering, cloud formation, and heterogeneous chemical reactions, and are thus a key element in the global climate system (Haywood and Boucher, 2000; Ravishankara, 1997). Important contributions to atmospheric particle number concentration are made by the homogeneous nucleation of supersaturated vapours. The feedback of this process on global climate is highly uncertain, although potentially large and opposite to the warming effect of greenhouse gases (Houghton et al., 2001). The formation of new particles by gas-to-particle conversion has been extensively studied in the remote marine and Arctic environment (Covert et al., 1992; Raes, 1995; Wiedensohler et al., 1996; Weber et al., 1999), in the free troposphere (Clarke, 1993), and in continental regions (Weber et al., 1997). In coastal regions a source related to biogenic iodine emissions has been identified (O'Dowd et al., 2002a). In the well-mixed continental boundary layer, particle formation is typically observed to be followed by subsequent particle growth occurring in relatively homogeneous air masses extending over large areas (Mäkelä et al., 1997; Hõrrak et al., 1998; Birmili and Wiedensohler, 2000; Nilsson et al., 2001a). Several model pictures describing particle nucleation and growth have emerged from the research of the past decade: (1) involvement of ammonia in the nucleation process, in addition to H_2SO_4 and H_2O (ternary nucleation; Coffman and Hegg, 1995), (2) ubiquitous existence of thermodynamically stable clusters, formed by ternary nucleation (Kulmala et al., 2000), with particle growth probably being dominated by oxidation products of biogenic organic

vapours such as terpenes or amines (O'Dowd et al., 2002b), (3) ion-induced or ion-mediated nucleation and growth (Yu and Turco, 2000), (4) enhancement of nucleation by small-scale turbulent atmospheric mixing (Easter and Peters, 1994; Nilsson and Kulmala, 1998), (5) enhancement of nucleation by atmospheric waves in stratified air (Nilsson et al., 2000). However, no physical model has currently been validated for a wide range of atmospheric conditions. The acquisition of new knowledge is mainly deterred due to the scarcity of long-term studies, and present instrumental shortcomings such as the inability to count freshly nucleated particles (< 3 nm), and to determine their chemical composition. Moreover, sensitive and high-time-resolution techniques have been missing to measure precursor gases (e.g. H_2SO_4, NH_3, organics) at accuracies required for atmospheric studies.

In the Hohenpeissenberg Aerosol Formation Experiment (HAFEX), recently developed techniques were simultaneously applied for the first time to measure atmospheric concentrations of H_2SO_4, OH, terpenes and aromatic hydrocarbons and to investigate the potentially important roles of these compounds in the formation and growth of new particles. The results are unique in that they are based on a combination of these measurements over the course of 2.5 years.

2 Experimental

2.1 Measurement site and program overview

The HAFEX measurement program was conducted at the Meteorological Observatory Hohenpeissenberg (MOHP; 47° 48′ N, 11° 07′ E), a Global Atmosphere Watch (GAW) site and mountain station operated by the German Weather Service (DWD). The observatory is located on top of the Hohenpeissenberg mountain (980 m above sea level) and about 300 m above the surrounding countryside. The nearest major city, Munich, is distant at ca. 60 km. MOHp is surrounded mainly by forests and agricultural pastures with coniferous trees and beeches growing on the slopes of the Hohenpeissenberg mountain in most directions. Air was sampled through inlets at 10 m above ground level, roughly corresponding to the height of the canopy. Particle size distributions, sulphuric acid and OH concentrations were measured continuously between 1 April 1998, and 3 August 2000, with occasional interruptions due to maintenance. Terpenes and hydrocarbons were measured on an hourly basis during specific periods and once a day whenever possible. During a 6-week period in April and May 1999, the particle size distribution was additionally measured at a second field station at the foot of the Hohenpeissenberg mountain. The horizontal and vertical distances between the two sites were approximately 3 km and 300 m, respectively. The long-term study was also supported by routine meteorological and atmospheric chemical measurements at MOHp, as part of the GAW program

(WMO2003), regular radiosonde ascent data from DWD's station at Munich, and back trajectories.

2.2 Particle number size distributions

Particle number size distributions (3-800 nm) were continuously recorded over 10–15 min intervals with a Twin Differential Mobility Particle Sizer (TDMPS) (Birmili et al., 1999). The TDMPS system is based on two Vienna-type differential mobility analysers (DMAs) (Winklmayr et al., 1991). Monodisperse particles were counted downstream of the DMAs with condensation particle counters (CPC; models UCPC 3025A and CPC 3010, respectively; TSI Inc., St Paul, MN, USA). Ambient air was sampled at 16.7 $1 min^{-1}$ through a PM_{10} Anderson impactor inlet and stainless steel tubing. Inversion of mobility into size distributions accounted for the bipolar charge distribution, and empirically determined transfer functions of the DMAs and CPCs. Particles were additionally counted using two stand-alone CPCs having different lower particle size detection limits (TSI models 3025A and 3010, respectively). In the TDMPS, particles were dried and classified at relative humidities below 10%. To reconstruct a particle size distribution at ambient relative humidity (RH), a hygroscopic growth model was applied relating the "wet" and "dry" particle sizes at given RH:

$$D_p(\text{RH}) = D_{p,0} \cdot (1.0 + 0.05 \cdot (1 - \text{RH})^{-1}) \tag{1}$$

The coefficients of this equation were determined from measurements of particle hygroscopicity with a Tandem Differential Mobility Analyser at Hohenpeissenberg in 1997 and 1998 (Karg et al., 1999). Equation (1) refers to the "more hygroscopic" fraction of aerosol particles (the dominating number fraction at Hohenpeissenberg), and was derived from data based on 50 nm particle size. Equation (1) deviates from that most frequently found in literature (Swietlicki et al., 1999), but we chose the present form because it provided a superior fit to the experimental data. In our paractice, the highest possible value of the growth factor $D_p/D_{p,0}$ was 1.83, corresponding to the upper limit 94% of the RH sensor.

2.3 H_2SO_4 and OH

Gas phase H_2SO_4 and OH concentrations were measured by atmospheric pressure chemical ionisation mass spectrometry (AP/CIMS) (Berresheim et al., 2000). Briefly, OH radicals were titrated by excess $^{34}SO_2$ to form $H_2^{34}SO_4$. Both $H_2^{34}SO_4$ and ambient H_2SO_4 ($\approx 96\%$ consisting of $H_2^{32}SO_4$) were chemically converted to the corresponding HSO_4^- ions by reaction with NO_3^- ions. A measurement cycle typically consisted of 20 min of continuous H_2SO_4 measurements (30 sec time resolution), followed by 5–10 min of OH measurements. For 5 min signal integration, conservative estimates of the detection limits of H_2SO_4 and OH were $3 \cdot 10^4$ and $5 \cdot 10^5$ molec. cm^{-3}. The overall accuracy (2σ) of the method was estimated to be 39% and 54%, respectively.

2.4 Monoterpenes and aromatic hydrocarbons

Monoterpenes and aromatic hydrocarbon (C_6-C_{10}) concentrations in ambient air were measured on-line by gas chromatography ion-trap mass spectrometry (GC-MS, Varian, Palo Alto, CA). Details of the system are to be presented in a future paper. Briefly, air samples were taken from a permanently flushed glass sample line (length: 10 m, ø 4 cm) and passed through a sodium thiosulfate ($Na_2S_2O_3$) impregnated glass fibre filter to remove ozone. Hydrocarbons were adsorbed in a Carbopack B (Supelco) trap at 40°C, desorbed at 230°C, and cryo-focussed in a silco-steel capillary (ø 0.28 mm) at 77 K. After thermal flash-desorption at 180°C hydrocarbons were separated on a capillary column (BPX-5, length: 50 m, ø 0.22 mm, 1 μm film) and detected by MS. The detection limits were below 2 pptv for air samples of 1.5 liters. The experimental measurement uncertainties were better than ±30% for aromatics, and ±30–50% for monoterpenes. Daily samples were taken at approximately 13:00 LT, and more often during intensive measurement periods. The above experimental set-up was used from the year 2000. During the years 1998–99, different adsorbent material (Carbopack C) and desorption procedures were used which caused additional losses and interconversion between different terpenes. Therefore, all aromatic hydrocarbon data shown in this paper refer to the entire HAFEX period, but terpene data only to the year 2000.

3 New particle formation events: Observations

3.1 Three case studies

Figure 1 shows three examples of new particle formation (NPF) including the time evolution of the particle size distribution, ultrafine particle (UFP) concentrations (size range 3–11 nm), total particle, H_2SO_4 and OH concentrations. The examples illustrate the dynamic range of NPF "events" that occurred during the 2.5 year measurement period. Indeed, we observed a continuum of observations, ranging from pronounced NPF events (Fig. 1, 15 May 1998) to such phenomena that are on the limit of being classified as "event" (Fig. 1, 7 April 2000). The concentrations of ultrafine particles (UFP) were generally low at night-time; no single particle formation event occurred during darkness. In the case of particle formation events, high UFP concentrations occurred predominantly around noon (median: 12:53 LT; quartile range: 11:53–13:45 LT). UFP concentrations peaked around 30 000 cm^{-3} (15 May 1998), 6000 cm^{-3} (25 March 1999), and 2000 cm^{-3} (7 April 2000). H_2SO_4 and OH showed pronounced diel cycles as well, with maximum concentrations between 1 and $2 \cdot 10^7$ cm^{-3} around noon in the cases shown in Fig. 1. During NPF events, the diameters of maximum particle concentration often shifted from initially 3–8 nm to larger diameters over several hours, occasionally

approaching 20 nm or more on the same day. This shift was clearly evident on 15 May 1998, although less pronounced on 25 March 1999 and 7 April 2000. Due to the regularity of this observation, this diameter shift is assumed to be the result of condensational growth of freshly nucleated particles over a large area. A third feature of NPF events was that after passing through the concentration maximum the concentration of UFPs decreased again, at an average characteristic time (decrease to $1/e$) of 2.4 h (full range: 0.4–6.4 h). A major process responsible for the removal of UFPs at Hohenpeissenberg is coagulation with larger particles (Birmili et al., 2000).

3.2 Particle formation events: spatial extension

Knowledge about the spatial scale of NPF events as a meteorological phenomenon can be helpful in the search for the possible particle sources. Here, we estimated the horizontal extension of air parcels in which NPF events occurred by multiplying the time during which a clear trace of the nucleation mode diameter could be seen, and the locally measured wind speed. This yielded an average extension of 87 km (minimum: 6 km, maximum: 339 km) suggesting that the NPF events in the central European source region extend over the mesoscale. Since at a fixed measurement site the full extent of these air masses might not be captured, we consider the range of a few 100 km as a lower estimate.

In a attempt to characterise the spatial homogeneity of NPF events, particle size distributions were measured concurrently at MOHp (980 m) and a second site at the foot of the Hohenpeissenberg mountain (680 m). Figure 2 shows the evolution of a NPF event, manifested by two separate waves just after 10:30 and 12:00 LT, which were detected simultaneously at both sites. The horizontal wind speed was 5 ± 1 m s^{-1}, blowing perpendicularly to the line connecting the two sites. The particle size distributions and total particle concentrations evolved in a very similar fashion at both sites (separated 3 km horizontally and 300 m vertically), demonstrating a relatively uniform spatial distribution of the NPF event in the inhomogeneous terrain around Hohenpeissenberg.

3.3 Shape of the particle size distributions

The shape of the particle size distribution during NPF events can be seen in Fig. 3: The maxima in the size distributions were always between 5 and 10 nm with decreasing concentrations towards smaller sizes. In particular, this is not an effect of the logarithmic scaling of D_p. While such "closed" distributions during or after atmospheric particle bursts have been observed by other research groups using very similar TDMPS systems (e.g. Mäkelä et al., 2000; Coe et al., 2000), measurements in an urban atmosphere in Atlanta have yielded particle size distributions that monotonically increase towards smaller particles (McMurry et al., 2000), which is
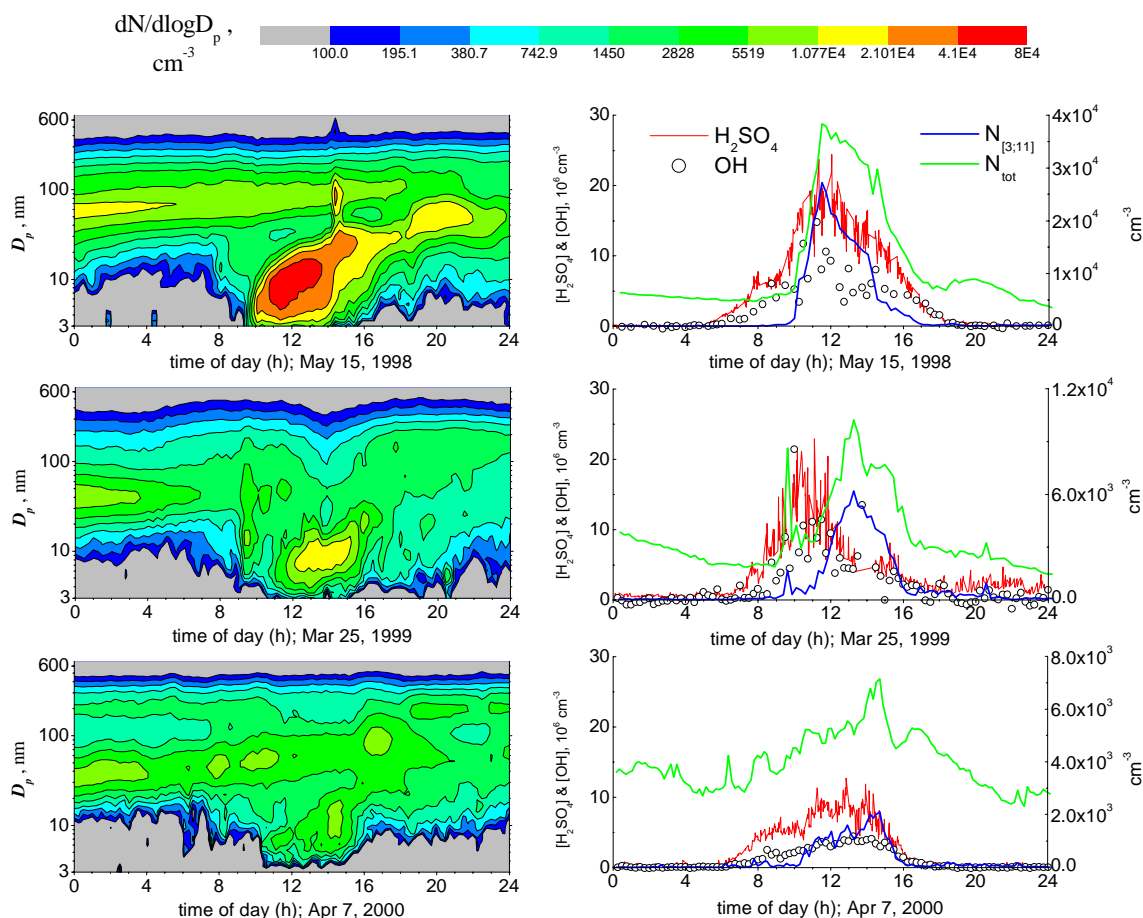
Fig. 1. Three days illustrating different intensities of new particle formation events at Hohenpeissenberg. Diurnal evolution of the particle number size distribution (left), UFP ($N_{[3;11]}$, total particle number (N_{tot}), H_2SO_4, and OH concentrations (right).

the shape theoretically expected from continuous nucleation. To scrutinise the possible impact of measurement artefacts in UFP range on our measurements we deployed, during much of the duration of HAFEX, a combination of two condensation particle counters (CPCs) using different lower detection limits ($\sim$3 and 11 nm, respectively). This allowed to determine particle concentrations independently from the TDMPS. Figure 4 shows data of an event on 26 December 1998, where the particle concentration profiles derived from both systems, including UFP concentrations, agreed within 10%. The measurement uncertainty of the TDMPS technique includes at least the following uncertainties: CPC counting efficiency, $\sim$10% (after individual calibration of an instrument); DMA transfer function, $\sim$20% (e.g. Reischl et al., 1997; Birmili et al., 1997); bipolar charge distribution, $\sim$20% (Wiedensohler, 1988). These estimates refer to the accuracy of a concentration measurement at the size 5 nm. Taking into account that CPC technology is more simple and less prone to possible nano-particle losses than the electrical classifier, we found no evidence to suggest that the mea-

sured closed nano-particle size distributions during HAFEX would be incorrect. Significantly, the size distributions during NPF events were closed for all wind directions. Another interesting finding was that the size distributions during NPF events were not significantly different in different seasons of the year. A discussion on the possible implications of these findings is provided in Sect. 7.
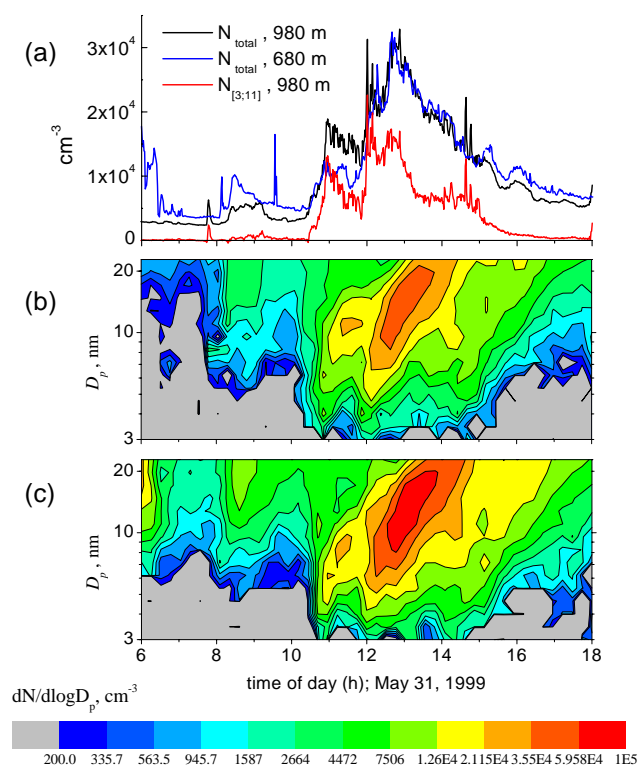
4 New particle formation events: classification and correlations with atmospheric parameters
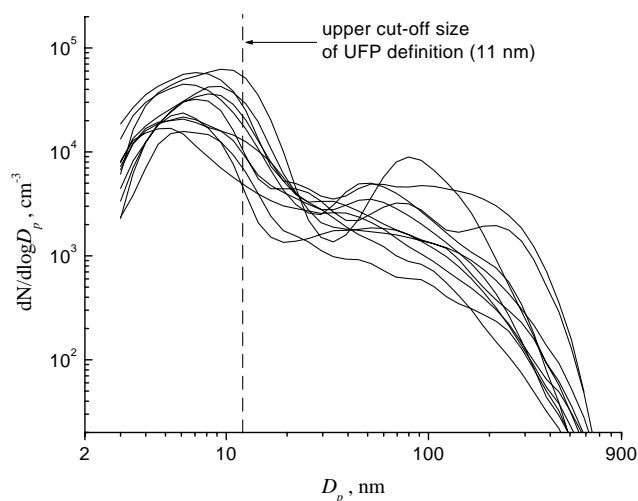
4.1 NPF event classification

For a systematic evaluation of the 2.5-year data set, we defined the occurrence of new particle formation "events" based on the time histories of ultrafine (3–11 nm) and total particle ($\geq$ 3 nm) concentrations ($N_{[3;11]}$ and N_{tot} hereafter). $N_{[3;11]}$ and N_{tot} were usually determined by numerical integration from the measured particle size distributions. Figure 5 illustrates three major characteristics of a diurnal

Table 1. Criteria for NPF event definition, based on parameters derived from the diurnal cycles of $N_{[3;11]}$ and N_{tot}.

	Parameter Name	Range	Parameter is indicator of
(a)	plateau concentration of $N_{[3;11]}$	$> 1000\ \text{cm}^{-3}$	particle formation intensity
(b)	time for $N_{[3;11]}$ to increase	< 4 hours	significant diurnal cycle in $N_{[3;11]}$
(c)	time for $N_{[3;11]}$ to decline	< 7 hours	significant diurnal cycle in $N_{[3;11]}$
(d)	fraction of UFPs ($N_{[3;11]}/N_{tot}$)	> 0.15	significant particle formation

Fig. 2. A new particle formation event (31 May 1999) observed simultaneously at two different levels of altitude: **(a)** Total particle and UFP concentrations at MOHP (980 m) and the low-level station (680 m), and evolution of the particle size distribution **(b)** at MOHP, and **(c)** at the low-level station.

Fig. 3. Particle size distributions measured during NPF events with high UFP fraction (> 0.58). The events shown date from 980401, 980407, 980420, 980515, 980519, 981226, 981108, 981228, 990103, 990106, and 990314.
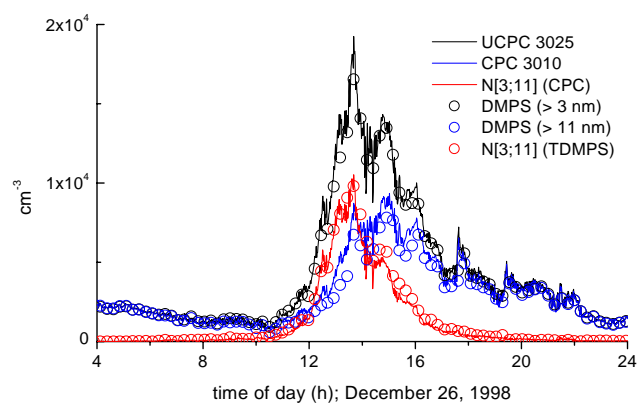
Fig. 4. Comparison between total and UFP number concentration derived from two CPCs with different lower detection limit, and the TDMPS, respectively. More data of this event is shown in Fig. 14.

cycle of $N_{[3;11]}$: (1) a rapid increase from low levels to near the daily maximum, (2) a plateau range where variations in concentration remain limited, and (3) a subsequent decline in $N_{[3;11]}$. By numerical curve fit, these characteristics were conveyed into four parameters that serve as a basis to classify all observed diurnal profiles into events and non-events: (a) a "plateau" ($\approx$ daily maximum) concentration, (b) a characteristic time for the curve to rise, (c) a characteristic time for the curve to decline, and (d) the fraction of UFPs during the event, i.e. the quotient $N_{[3;11]}/N_{tot}$. See Fig. 5 for an illustration of the parameters (a)–(c). To be classified as a NPF event, the parameters (a)–(d) of an individual diurnal cycle

had to satisfy the specific range criteria, given in Table 1. Next, the plateau (maximum) concentration (a) was used to categorise all NPF events into 3 classes (I, II, III) representing different UFP maximum concentrations: Event class I
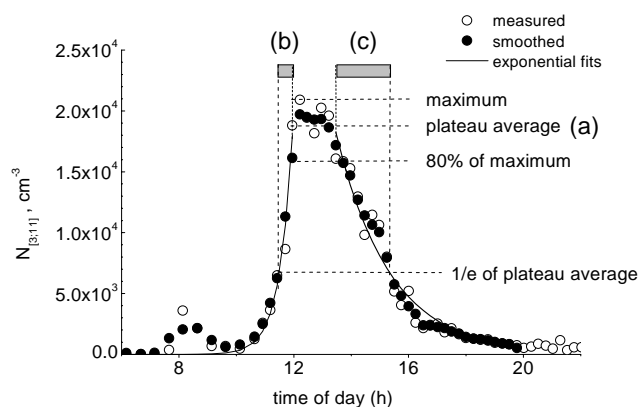
Fig. 5. Detection of new particle formation events based on the diurnal cycle of $N_{[3;11]}$. Data is from 20 April 1998. For explanation of the parameters **(a)**, **(b)**, and **(c)**, see Sect. 4.1.

Fig. 6. Seasonal frequency of different classes of NPF events at Hohenpeissenberg (April 1998–August 2000).

($> 7000\ cm^{-3}$), class II (2500–7000 cm^{-3}), and class III (1000–2500 cm^{-3}). The application of the above described schemes yielded 117 NPF events out of a total of 651 days, which means that particle formation events occurred on approximately 18% of all days. 19 events were ranked class I, 49 class II, and 49 class III. These numbers are shown in Fig. 6, keyed after the different seasons. NPF events occurred most frequently in winter (25% event probability) and spring (21%) but interestingly, least frequently in summer (12%). Particularly, no class I event was observed in summer, which was surprising with regard to the expectation that the photochemically produced vapour reservoir would be most intense in that season. Finding a high seasonal event frequency in spring is shared by other statistical descriptions of NPF events over continental areas (Mäkelä et al., 2000; Birmili and Wiedensohler, 2000; Hõrrak et al., 2000), but a frequent occurrence of wintertime events such as at Hohenpeissenberg has not been reported yet.

4.2 Variations of H_2SO_4, OH, meteorological parameters, and the condensational sink

Median diurnal cycles of H_2SO_4 and OH concentrations and meteorological parameters were calculated (see Fig. 7). Because of the seasonal influence of boundary layer convection, the data were divided into two blocks comprising the "warm" season (March–October) and the "cold" season (November-February), respectively. In the warm season, H_2SO_4 concentrations correlate with the intensity of NPF events (Fig. 7). The highest event class (I) shows daily maximum H_2SO_4 concentrations above 10^7 molec. cm^{-3}, whereas the event classes II and III were associated with peak concentration of $5 \cdot 10^6$ and $3 \cdot 10^6\ cm^{-3}$, respectively. Event class III concentrations were similar to non-event concentrations. The cold season was different in that H_2SO_4 typically peaked between 6 and $8 \cdot 10^6\ cm^{-3}$ for all event classes (I-III) whereas on non-event days, only $\sim 2 \cdot 10^6\ cm^{-3}$ were measured. Al-
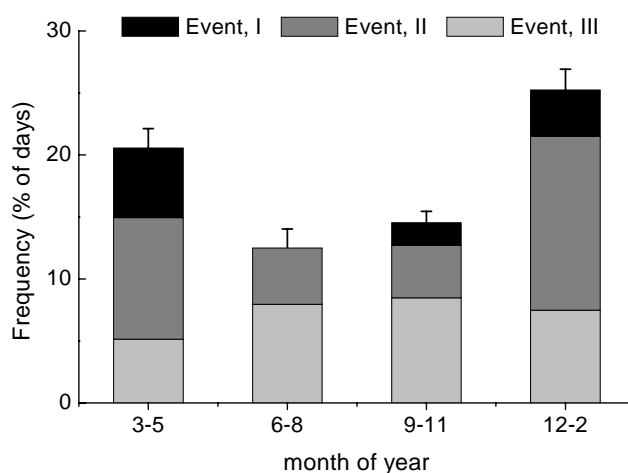
though the hydroxyl radical (OH) concentration showed a pronounced seasonal behaviour — with daily maxima typically around $\sim 4 \cdot 10^6\ cm^{-3}$ in the warm season, but only $2 \cdot 10^6\ cm^{-3}$ in the cold season — it shows less distinction between event and non-event days. An notable exception is event class I in the warm season when OH concentrations reached up to $7 - 8 \cdot 10^6\ cm^{-3}$ between 09:00 and 12:00 LT. In order to make a seasonally invariant distinction between cloudy days and clear skies, each daily solar irradiance cycle was normalised by a cloudless reference profile. Reference profiles were obtained by averaging the 3 profiles of a particular month of the year that showed the most amount of radiation. A radiation value of 1 accordingly refers to a clear sky. Figure 7 shows that the particle formation intensity correlated with solar irradiance, and anti-correlated with relative humidity (RH). Both features were especially pronounced in the cold season. While the correlation with solar irradiance is plain to understand in terms of photochemical processes being responsible for the generation of gaseous precursors, the anti-correlation with RH is less evident. In fact, nucleation theory rules that particle formation be enhanced by *high* relative humidities. Profiles of absolute humidity (see Fig. 7) suggest that in the warm season it was largely a low absolute humidity which caused the low RH and particularly, not excessive temperatures. In the cold season, there was a also significant contribution of warm temperatures (warm air advection) leading to the low RHs observed during NPF events of classes I and II. Since humidity is no independent factor (it correlates with cloudiness), the physical interpretation of this factor in relation to particle formation is not clear.

A further factor related to the formation of new particles is the pre-existing particle surface area, which is also RH dependent. The pre-existing particle surface area competes with the particle nucleation process for condensable vapours. The measure for this competition is the "condensational sink
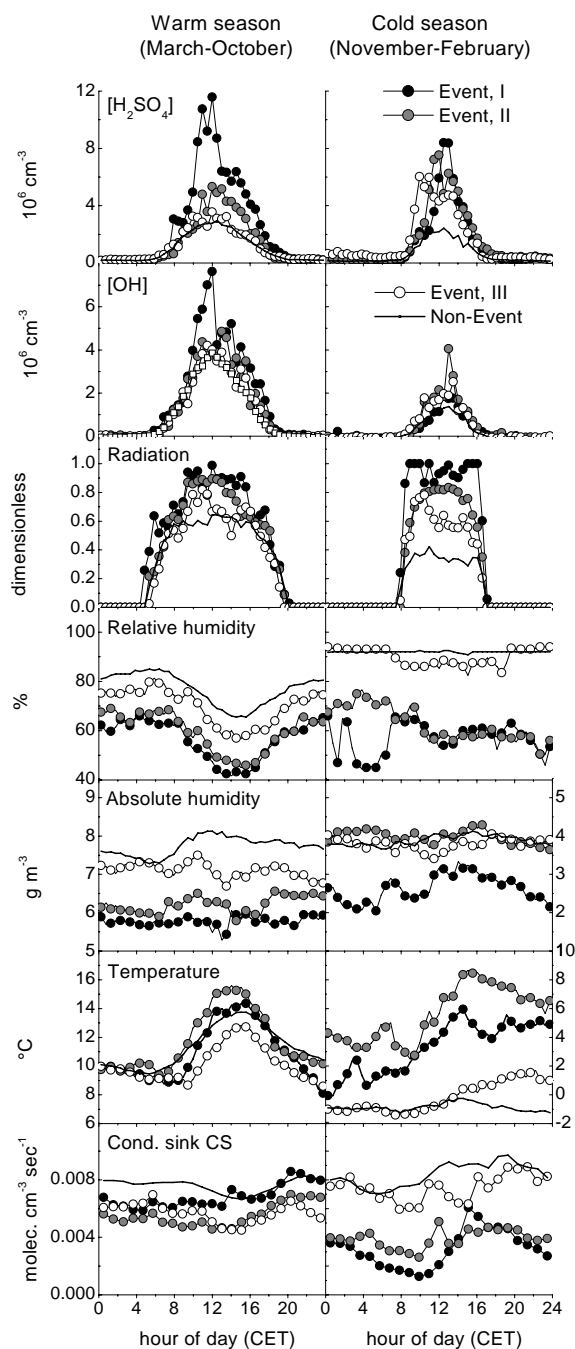
Fig. 7. Median diurnal cycles of [H$_2$SO$_4$], [OH], normalised solar irradiance, relative humidity (RH), absolute humidity, temperature ($h = 2.0$ m) and the condensational sink CS (mean values), separated after different particle formation intensities. Solar irradiance data were seasonally normalised (see text for details). RHs > 94% was the upper limit of the RH sensor.
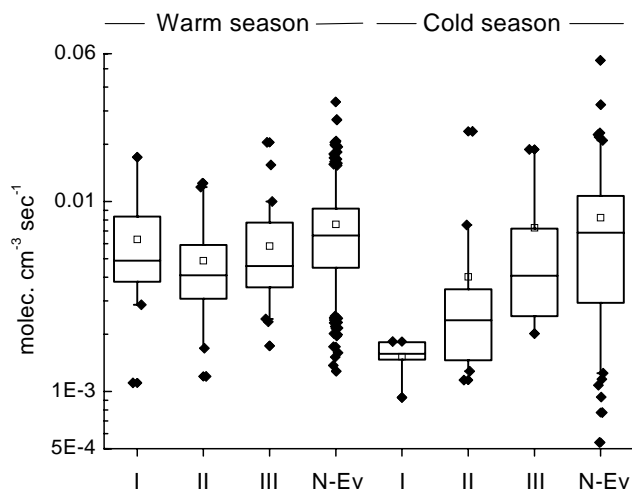

Fig. 8. Box-and-whisker plot of the values of the condensational sink CS (10:00–12:00 LT CET), for NPF events (classes I, II, III) and Non-events (N-Ev). Box indicates median and quartiles, open squares indicate mean, and whiskers indicate the 5–95% range. Solid diamonds represent outliers outside the 5–95% range.

ity using the hygroscopic growth model from Sect. 2.2. The mass transfer equations included the Dahneke Kernel (Seinfeld and Pandis, 1998), H$_2$SO$_4$ molecular diffusivity at ambient temperature, an accommodation coefficient of unity. The diurnal cycles of CS$_{wet}$ as a function of the NPF event class are displayed in Fig. 7, bottom graph. In the warm season CS$_{wet}$ was typically 20% lower on NPF event days compared to non-event days, which is a weak indication of an inhibitive effect of the pre-existing particle population on the particle formation process. More significance is given in the cold season where CS$_{wet}$ is lower by up to 80% on event days. This anti-correlation between particle formation intensity and preexisting condensational sink in the cold season can again be clearly seen in Fig. 8. Owing to the wide scatter in values of CS, however, no critical threshold for CS could be defined, above which no events occur.

The consideration of anthropogenic tracers (mixing ratios of CO, NO, not shown) suggested that the low CS$_{wet}$ on class I and II events in the cold season (cf. Fig. 7; before 10:00 LT) were the result of the MOHp mountain site residing in a clean layer of air above the surface inversion, showing a lower pre-existing particle population. Further evidence indicated the advection of south-westerly or southerly warm air masses during these events, originating mostly from Southern France and the Mediterranean (class I: 5 out of 5; class II: 15 out of 19). Being ca. 30 km north to the Alpine mountain range, the Hohenpeissenberg site is then prone to be influenced by Foehn or *Foehn-like* conditions, which can lead to the subsidence of air in wave packets, or stress-induced mixing by breaking lee waves. These phenomena, which would be favourable for the formation of new particles were, however, difficult to assess using the limited
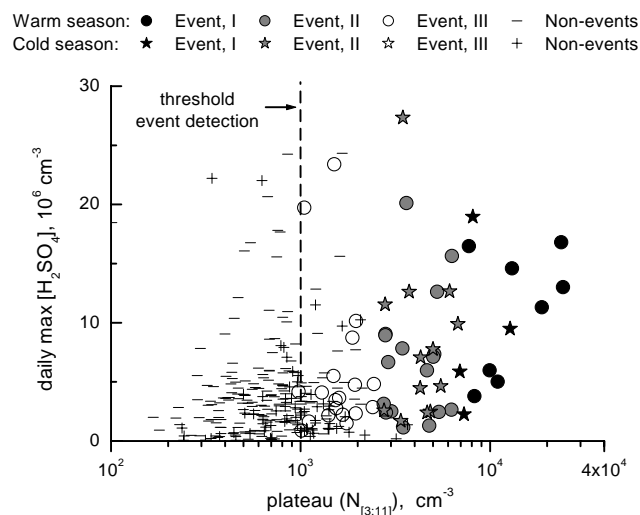
flux" (CS$_{wet}$) of condensable vapours onto the pre-existing particles population. CS$_{wet}$ was calculated with the measured particle size distribution adjusted to ambient relative humid-

Fig. 9. Cross-correlation between the UFP plateau and daily peak H_2SO_4 concentrations.

Fig. 10. Daily peak concentrations of vapour availability X_{norm} vs. normalised solar irradiance. Only data from the cold season was used. The dashed rectangle describes a parameter space that encompasses 90% of all class I-II events, while only allowing for 6% of the non-events.

spatial information available to this study. The back trajectories used probably also lack accuracy in this strongly inhomogeneous terrain (Georgelin et al., 1997) and prevent confident localisation of the source regions of these air masses. We can therefore not decide if the low particle surface area alone, or the mentioned orography-related phenomena were responsible for the observation of the associated NPF events.

4.3 Statistical significance of the relation between NPF events, H_2SO_4 and solar irradiance

The relationship between the particle formation intensity and H_2SO_4 was examined with statistical tests. To ease statistical treatment, daily maximum values of H_2SO_4 and solar irradiance were determined by fitting Gaussian curves to each daily cycle. These daily maximum values were then compared to the observed UFP maximum concentration (i.e. the plateau values of $N_{[3;11]}$), as can be seen in Fig. 9 for H_2SO_4. The statistical confidence that event days are linked with increased H_2SO_4 was 99.99% for class I events, 99% for class II events but less than 90% and, thus, not significantly for class III events (see Table 2). Before testing the same hypothesis on solar irradiance, the diurnal cycles of solar irradiance were normalised by a cloudless radiation profile of the respective month (cf. Fig. 7) in order to better distinguish between cloudy and clear days over the entire annual cycle. While the solar irradiance intensity was less significantly correlated to the observed UFP maximum concentrations without normalisation, it proved to be a superior indicator of particle formation for all event classes I-III including this normalisation (see Table 2). Despite NPF events being significantly associated with increased H_2SO_4 and solar irradiance, the wide scatter in data such as H_2SO_4 for the class I (cf. Fig. 9) clearly demonstrates that there is no lower thresh-
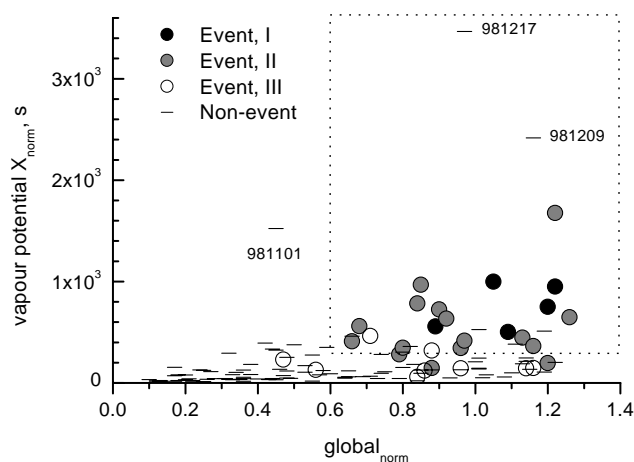
old criterion in H_2SO_4 that would trigger a NPF event. Indeed the lowest H_2SO_4 peak concentration observed during a class I event (27 January 2000) was as low as $2.8 \cdot 10^6$ cm^{-3}. A similar scatter of data involving similar conclusions was observed in case of solar irradiance.

4.4 The concept of vapour availability

Based on the findings of the previous sections we extend the analysis to condensable species of photochemical origin in general (with vapour pressures similar to H_2SO_4), and introduce the quantity "vapour availability" X. A similar approach was proposed by (Clement et al., 2001) to study the onset and cut-off criteria of NPF events at a Finnish boreal forest site. The vapour availablity X is defined as

$$X = \text{solar flux} / CS_{wet}, \qquad (2)$$

CS_{wet} being the condensational sink flux of condensable vapours described above. Equation (2) is the variant of a steady-state mass balance equation, balancing a source and a sink term of a photochemically produced condensable vapour, resolved after X, the latter therefore representing an equilibrium vapour concentration. Figure 10 compares the daily peak values (determined by Gaussian fits as in the preceding section) of the vapour availability X_{norm} and the monthly normalised solar irradiance (cf. Fig. 7). By requiring $X_{norm} > 280$ s and $Global_{norm} > 0.6$ (see Fig. 10), a parameter space could be defined that encompasses 90% of all class I-II events, while only allowing for 6% of the non-events. This relatively powerful separation resulted solely for the cold season data. In the warm season no such parameter space could be established, suggesting that in that the evolution of NPF events depends less critically on the shown com-

Table 2. Mean daily fit maximum values of the parameters global radiation, solar irradiance (seasonally normalised), and H_2SO_4 for different event classes. p_0 indicates the maximum error probability at which the hypothesis H_0: $\mu_{x,i} > \mu_{x,0}$ is accepted (one-sided two-sample Gauss test).

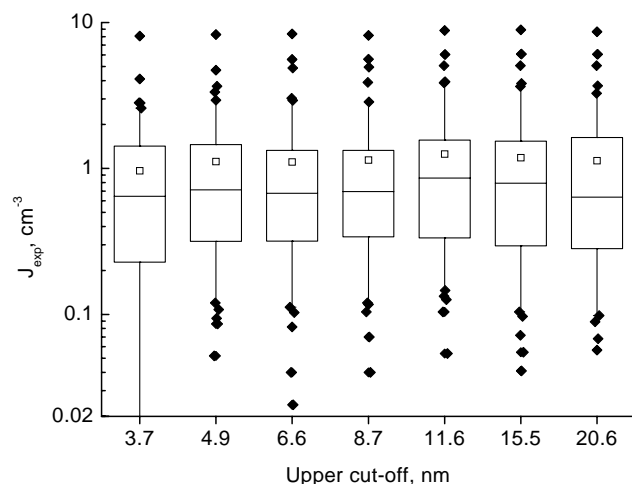| | H_2SO_4, cm^{-3} | | | solar irradiance, $W\,m^{-2}$ | | | Global Rad. (normalised) | | |
	μ_x	$\sigma(\mu_x)$	p_0	μ_x	$\sigma(\mu_x)$	p_0	μ_x	$\sigma(\mu_x)$	p_0
Non-Events	4.10	0.28		504	13		0.69	0.013	
Event, I	10.29	1.57	0.9999	682	56	0.9988	0.89	0.034	0.9999
Event, II	7.46	1.08	0.9985	602	31	0.9983	0.89	0.020	0.9999
Event, III	5.57	1.15	0.8893	528	37	0.7234	0.78	0.036	0.9908

Fig. 11. Box-and-whisker plot of various experimental particle formation rate definitions, i.e. as a function of different upper size cut-offs defining the range of UFPs. Box indicates median and quartiles, open squares indicate mean, and whiskers indicate the 5–95% range. Solid diamonds represent outliers outside the 5–95% range.

bination of high solar irradiance and low pre-existing particle population.

5 Estimates of the particle formation rate

5.1 Experimental results

Particle formation rates were experimentally determined by dividing an observed increase in particle number concentration by the elapsed time: $J_{exp} = N_{UFP}/\Delta t$ (e.g. Weber et al., 1997). Doing so requires the assumption of spatial atmospheric homogeneity; then, the observed increase in particle concentration > 3 nm can be considered as a temporally shifted "image" of the original nano-particle burst. Experimental (or "apparent") formation rates J_{exp} were calculated for different UFP size ranges, marked by upper size cut-offs 3.6, 4.9, 6.6, 8.7, 11.6, 15.5, and 20.6 nm. (The lower size cut-off was always 2.8 nm, i.e. the lower detection limit of

the TDMPS). Figure 11 shows the resulting formation rates, which were mostly in the range 0.1–3 $cm^{-3}\,s^{-1}$. Notably, J_{exp} did not sensitively depend on the choice of the size interval, so we generally employ the rate definition based on the interval 3-11 nm, already introduced in Sect. 4.1 of this paper.

5.2 Ternary $H_2SO_4/NH_3/H_2O$ nucleation

Our question was: Can ternary homogeneous H_2SO_4-NH_3-H_2O nucleation serve as a model to explain the observed particle formation events at Hohenpeissenberg? The experimentally determined particle formation rate J_{exp} was therefore compared to a ternary nucleation rate of H_2SO_4, ammonia (NH_3) and H_2O, now available in parametrised form (Napari et al., 2002a,b). The ternary rate was first calculated for in-situ conditions, based on measurements of H_2SO_4, RH, temperature, and an estimate for NH_3. The nucleation rates were calculated during an interval from 30 min before the beginning of a formation event until the time the plateau of $N_{[3;11]}$ was reached (cf. also Fig. 5), and then averaged. For all calculations, the NH_3 mixing ratio was set to 100 pptV. On the one hand this is the nucleation parametrisation's upper limit of validity (Napari et al., 2002a). On the other hand it is consistent with the presence of significant sources of NH_3 around Hohenpeissenberg (intense agriculture; raising of livestock such as dairy cattle). No ammonia measurements were carried out during HAFEX, but we presume that the ammonia mixing ratios in the well-mixed boundary layer were comparable to those measured at a rural site in East Germany where an annual median of 6 ppbV was reported (Spindler et al., 2001). The comparison between the experimentally determined formation rates and the calculated ternary nucleation rates is presented in Fig. 12a: The experimental formation rates ranged between 0.01 and 9 $cm^{-3}\,s^{-1}$ while the ternary rates were scattered across the range $10^{-9} - 10^3$ $cm^{-3}\,s^{-1}$. Although no remarkable correlation between the two rates was found, the comparison in Fig. 12a leads to the conclusion that ternary nucleation is, in principle, able to generate the number of fresh nano-particles that are later observed as particles > 3 nm. This is in stark
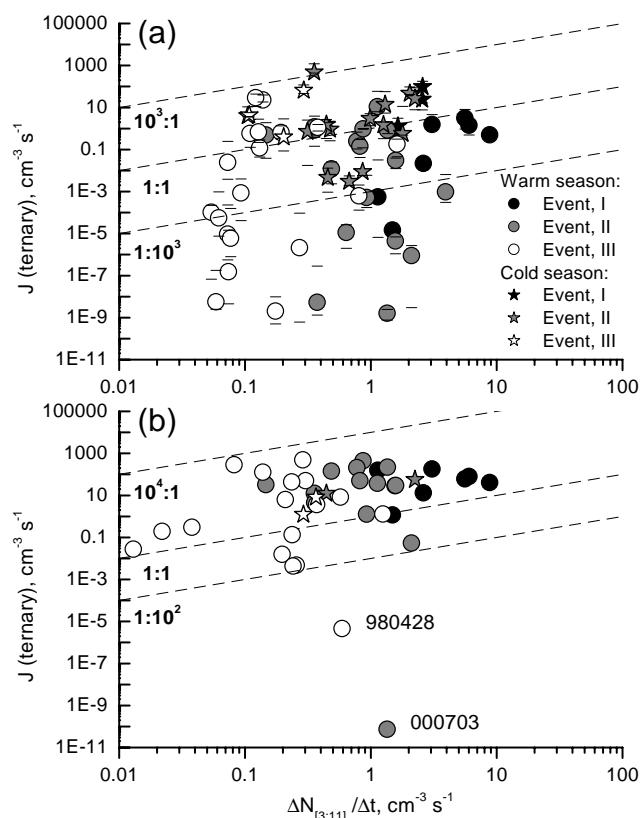
Fig. 12. Comparison between the "apparent" particle formation rate $\Delta N_{[3;11]}/\Delta t$ and the ternary (H_2SO_4-NH_3-H_2O) nucleation rate, based on measured $[H_2SO_4]$ and $[NH_3] = 100$ pptV. **(a)** is based on the thermodynamic conditions near the ground, **(b)** on those near the top of the boundary layer. Horizontal bars in (a) indicate the variability of J(ternary) during the course of NPF events. (b) includes cases with mixed layer height > 700 m only (cf. text).

contrast, e.g. to binary H_2SO_4-H_2O nucleation, where initial calculations yielded rates between 6 and 30 orders of magnitude lower (shown in the *ACP Discuss.* version of this paper).

5.3 Particle formation near the top of the boundary layer?

While the ternary rates above were calculated under the assumption of in-situ conditions near the surface, we now consider the thermodynamic conditions that prevail near the top of the boundary layer (TBL), where temperatures and relative humidities may be more favourable for nucleation (Nilsson et al., 2001b). The mixed layer height was estimated from the 13:00 CET radio sonde ascent at the DWD station Munich (70 km north-east of Hohenpeissenberg) using the simple parcel method and an excess temperature of 0.5 K (Holzworth, 1964). Temperature and RH were obtained from interpolation of the aerological data to that level. H_2SO_4 was assumed to be well mixed across the boundary layer depth and, as before, the NH_3 mixing ratio was assumed to be 100 pptV. Importantly, only cases were consid-
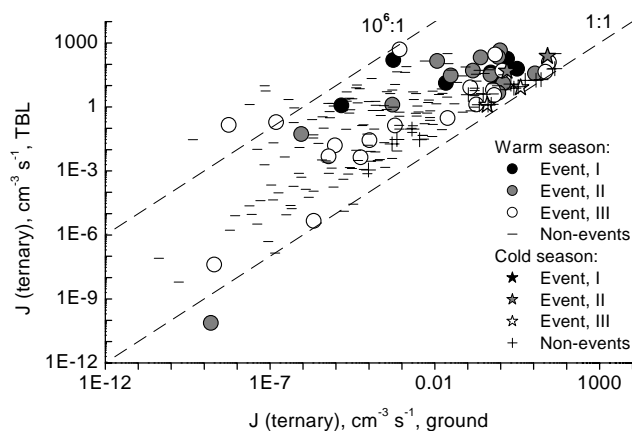

Fig. 13. Ternary H_2SO_4/NH_3/H_2O nucleation rates, based on the thermodynamic conditions near the ground (abscissa) and at the top of the boundary layer (ordinate). Assumptions include a uniformly distributed H_2SO_4 within the boundary layer, and $[NH_3] = 100$ pptV. Only cases with mixed layer height > 700 m are included (cf. text).

ered when the mixed layer height was greater than 700 m (44 out of 64; overwhelmingly cases from the warm season, i.e. the months March–October). This height corresponds to 1.5 times the vertical distance between the Hohenpeissenberg mountain and the radio sonde measurement site (in flat terrain), and ensures that the MOHp site was within the mixed layer. Figure 12b shows the comparison between the experimental particle formation rate, and the ternary nucleation rate under TBL thermodynamic conditions: The calculated ternary rates were scattered around the experimental formation rates within a few orders of magnitude only. 95% of the data points showed an agreement within a factor range of 10^{-2}–10^4 (Fig. 12b). The two outlying points in Fig. 12b are explained by relatively low H_2SO_4 concentrations. As can be seen in Fig. 13, the ternary nucleation rate predicted near the TBL may be up to 6 orders of magnitude higher than that near the ground. Despite the agreement shown, however, we advocate care in the interpretations of these results, especially in view of the assumptions made on the unknown precursor concentrations near the TBL.

Still, it remains unexplained why NPF events actually do not happen on many more days. Figure 13 suggests that on many non-events, the ternary H_2SO_4-NH_3-H_2O nucleation rate was also on order of 1 cm^{-3} s^{-1}. The overall mean values of the ternary nucleation rate are higher on event days compared to non-event days but, again, no satisfactory threshold criterion could be defined to effectively separate the two fractions (similarly to the consideration of H_2SO_4 in Sect. 4.3). This also applied to attempts using the pre-existing condensational sink (except in the cold season; cf. Fig. 8) and logical combinations of both. The inability to separate events from non-events by combinations of parameters based on the measurements, or such derived thereof,
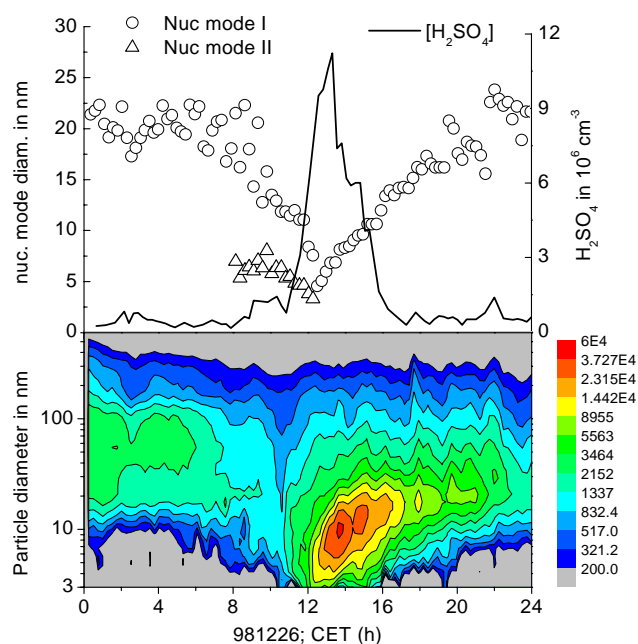
Fig. 14. Time series of the particle size distribution ($dN/d\log D_p$ in cm^{-3}), the nucleation mode diameter, and H_2SO_4. Data is from 26 December 1998, a winter class I event day. The growth rate obtained from a linear fit was $2.1\,nm\,h^{-1}$.

shows that relevant parts of the process eventually leading to a NPF event are still not understood.

6 Estimates of the particle growth rate

6.1 Results derived from experimental observations

During HAFEX, a growth of the nucleation mode particles was frequently observed over the course of several hours after the initial appearance of the mode (see Fig. 14). To quantify this effect, the particle size distributions were individually parametrised by multiple lognormal functions using a least squares algorithm, thus yielding a time series of the nucleation, Aitken, and accumulation mode diameter for each event. As illustrated in the example in Fig. 14, the diameter of the nucleation mode often increased in a closely linear fashion with time. From the theory of mass transfer in the free molecular regime, such a linear growth indicates a nearly constant concentration of condensable vapours (Friedlander, 2000). Experimentally, the time of linear particle growth mostly coincided with the time when H_2SO_4 was near its daily peak. Occasionally, however, the growth was observed to continue beyond that period (see Fig. 14, after 16:00 LT), a phenomenon that is unlikely to be explained by the condensation of short-lived photochemically produced vapours with a symmetric diurnal cycle around noon. Although linear growth behaviour was occasionally observed for particles as large as 20 nm, the linear fit concentrated on the data in the
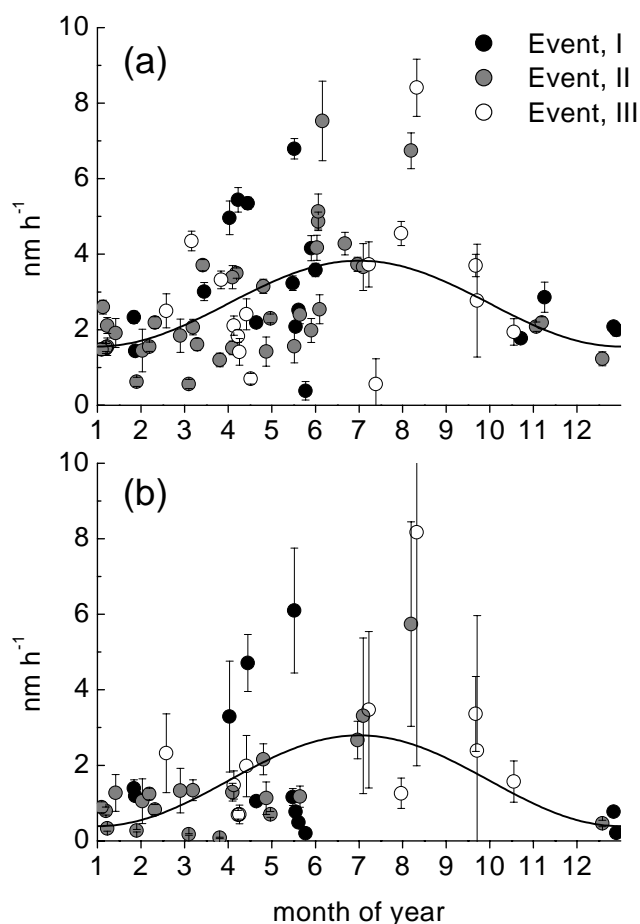

Fig. 15. Annual distribution of **(a)**, the experimentally determined growth rate of nucleation mode particles and **(b)**, the excess particle growth rate after subtraction of the term caused by H_2SO_4-H_2O-NH_3 condensation. Both graphs include a fit curve of the first harmonic.

lowest particle size range, 3–10 nm, i.e. as close as possible to the size of the critical particle embryos. Not all NPF events could be analysed by the method described above; particularly class III were excluded from the analysis because of low particle concentrations and the lack of a clear trace of the nucleation mode diameter with time. Figure 15a displays the annual distribution of the growth rates determined for 71 events evaluated. The entire range of growth rates spanned 0–$9\,nm\,h^{-1}$ with an overall mean of $2.6\pm0.2\,nm\,h^{-1}$. Importantly, the growth rates were limited during the months October to February ($\leq 3\,nm\,h^{-1}$), leading to a seasonal cycle with increased growth rates in summer (Fig. 15a). This observation is at first sight consistent with the stronger presence of vapour phase precursors as a result of enhanced photochemical activity but also increased organic precursor emissions from the biosphere. Furthermore, the general absence of correlation between the particle growth rate and the particle formation intensity in Fig. 15a may be seen as indicative
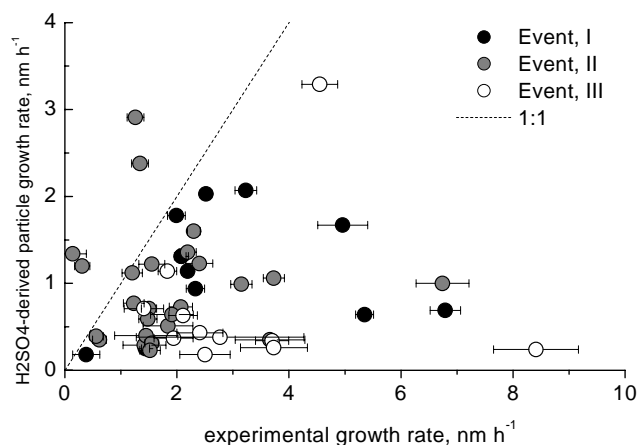
Fig. 16. Direct comparison between the experimentally and theoretically determined growth rate of nucleation mode particles.

of the existance of different vapour sources for particle nucleation and growth.

6.2 Particle growth by H_2SO_4-H_2O-NH_3 condensation

Since direct measurements of sulphuric acid were available, it was possible to estimate its contribution to the particle growth rate. Here, measured H_2SO_4 was assumed to co-condense with H_2O, being neutralised by NH_3 in a 2:1 molar ratio (Birmili et al., 2000). The limiting factor in the growth rate is assumed to be the diffusion of molecular H_2SO_4 onto the pre-existing particles at their ambient size. Ammonia is supposed to be sufficiently available: A hypothetical ambient mixing ratio of 6 ppbV (cf. Sect. 5.2) corresponds to roughly $2 \cdot 10^{11}$ cm^{-3} NH_3, which is 10^4 times more than the H_2SO_4 maximum concentration observed at Hohenpeissenberg. The calculated H_2SO_4-NH_3 rate was finally averaged over the time interval corresponding to the linear observed growth of the nucleation mode. Figure 16 shows the two growth rates for the 49 events when H_2SO_4 data were available. Overall, the two rates show little correlation, suggesting that the particle growth rates observed during HAFEX contain significant contributions from species other than H_2SO_4 and NH_3. Four points are to the left of the unity curve (Fig. 16) and were attributed to shortcomings in the nucleation mode diameter fit method or to limitations of the one-point observation. The overwhelming majority of data points are to the right of the unity curve, therefore allowing to describe the growth of the nucleation mode as a composition of one term describing H_2SO_4-NH_3 condensation (0.7 nm h^{-1} on average), and another term, a "missing growth rate", representing the difference between the two growth rates (1.9 nm h^{-1} on average). The annual cycle of the missing growth rate is shown in Fig. 15b. Most missing growth rates were between 0 and 2 nm h^{-1} being indicative of an additional source of condensable vapours throughout the year. 8 data points occurred
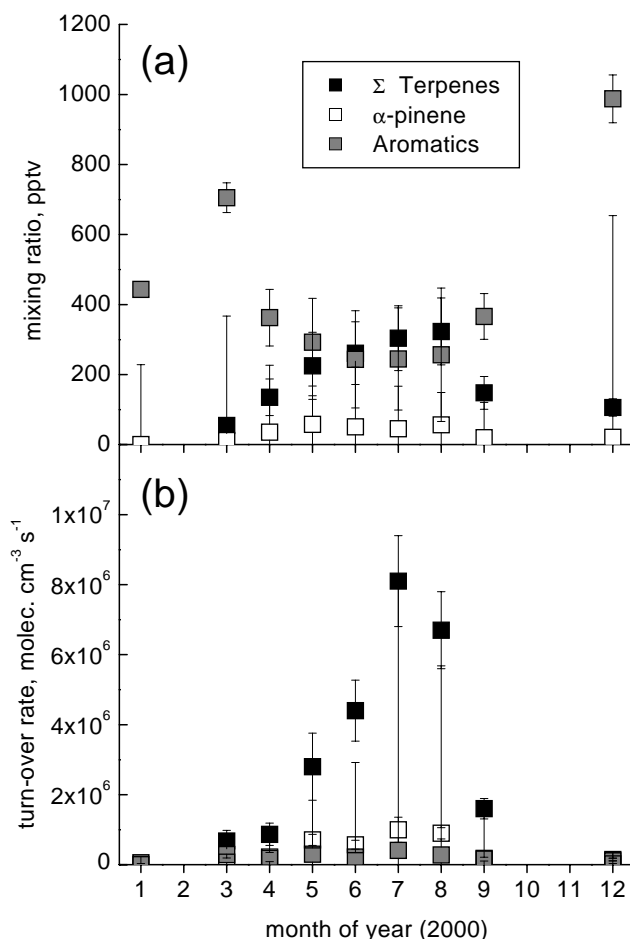

Fig. 17. **(a)** Monthly averages of the noontime (11:00–15:00 LT) mixing ratios of the sum of C_6-C_9 aromatic hydrocarbons (circles), α-pinene (triangles), and the sum of all measured terpenes (diamonds) including α-pinene, β-pinene, Δ^3-carene, eucalyptol, limonene, camphene, myrcene, sabinene, tricyclene (in order of abundance), and traces of α-terpinene, γ-terpinene and terpinolene; **(b)** the corresponding noon time turnover rates due to reactions with OH and ozone. In case of OH the measured concentrations were used, in September and December for lack of concurrent OH measurements monthly noontime averages were used. The bars represent one sigma standard deviations.

above 3.0 nm h^{-1}, notably all between April and September. These point to a source of condensable vapours, which would be predominantly active in the warm season.

6.3 Monoterpenes and aromatics

6.3.1 Measurements and turn-over rates

Figure 17a presents the seasonal cycles of monoterpene and aromatic hydrocarbon concentrations during HAFEX. Aromatic hydrocarbons were most abundant in winter and the least in summer. Since their seasonal cycle is inverse to that of OH (cf. Fig. 7), the calculated turn-over rates due to re-

actions with OH did not show a pronounced seasonal cycle (see Fig. 17b). Terpenes, in contrast, showed the highest mixing ratios in summer (Fig. 17a) due to their temperature-dependent biogenic source intensity (Guenther et al., 1993). Since OH and ozone concentrations also peak in summer, the highest turn-over rates were determined for the summer months, for instance $6.0 \pm 5.1 \cdot 10^6$ molec. $cm^{-3} s^{-1}$ in August. The winter values were generally below $2 \cdot 10^5$ $cm^{-3} s^{-1}$. Roughly two thirds of the turn-over rate were due to reactions with OH. Among all monoterpenes, α-pinene was the species with the highest mixing ratio and, in most months, highest turn-over rates. The turn-over rate of aromatics and monoterpenes can be used to roughly estimate the production rate of semivolatile organic compounds. Products from photooxidation of α- and β-pinene, such as pinonic acid, pinic, and norpinonic acid, have been identified in the aerosol phase in a number of chamber studies (Hoffmann et al., 1997) and recently in forest air (Kavouras et al., 1999). The results shown here suggest that the contribution of anthropogenic aromatics to aerosol formation is negligible compared to that of biogenic in the rural background air.

6.3.2 Potential contribution to particle growth

The HAFEX data indicates a general seasonal correlation between the production rates of biogenic aerosol precursors and the growth rates of newly formed aerosol particles: Both seasonal cycles show a maximum in summer (cf. Figs. 15 and 17b). Using the summer maximum of the monoterpene turn-over rate (which are a measure for the production rate of semivolatile products from photo-oxidation of terpenes) and the corresponding reaction yields of condensable products between 1 and 10% (Hoffmann et al., 1997), we determined mid-day production rates of semivolatile products in a range $6 \cdot 10^4 - 6 \cdot 10^5$ molec. $cm^{-3} s^{-1}$. These figures are up to 1 order of magnitude higher than the calculated production rates of H_2SO_4 from atmospheric SO_2 oxidation by OH, which were $< 5 \cdot 10^4$ $cm^{-3} s^{-1}$ on a monthly average. In conclusion, the potential growth rate of nucleation mode particles by condensation of semi-volatile organic species may easily exceed the growth rates based on H_2SO_4-NH_3; it is therefore a realistic candidate to account for part of the missing growth rate determined in Sect. 6.2. In an attempt to relate the missing particle growth rate (Fig. 15b) to the monoterpene turn-over rate, no significant correlation was obtained: At high turn-over rates exceeding $3 \cdot 10^6$ molec. $cm^{-3} s^{-1}$, the missing growth rates varied between 0 and 4 nm h^{-1}. With the number of data available being limited to 11 events, and considering the uncertainty of the assumptions made for the organic contribution to particle growth, a quantitative assessment of the contribution of biogenic compounds to particle growth could not be made here.

6.3.3 Potential contribution to new particle formation

A surprising result in Sect. 4.1 was that the seasonal distribution of NPF events at Hohenpeissenberg (cf. Fig. 6) was inverse to the seasonal cycle of terpene turn-over rates (Fig. 17b). Terpene turn-over rates peaked in the months July and August, but NPF events were largely absent during that period. Looking at individual days, we further found no evidence for significantly enhanced monoterpene turn-over rates on days with NPF events compared to non-event days. Both findings indicate that any direct contribution from potential biogenic aerosol precursors to new particle formation (i.e. nucleation) was either not detectable and/or negligible, or that other factors were more important in controlling the occurrence of NPF events.

7   Discussion of the closed particle size distributions

As shown in Sect. 3.3, the particle size distributions observed during the NPF events of HAFEX were "closed", i.e. the particle concentration of the nucleation mode in the range 3–8 nm decreased with decreasing particle size. If experimental uncertainties can be ruled out two possible scenarios can be thought of that would lead to a closed distribution: (1), particles were formed some time before their observation upwind the measurement site or (2), the growth rate of nucleation mode particles was non-linear with time; growth would be relatively fast just after nucleation, and decelerate with increasing particle size. With respect to the first hypothesis, newly formed particles could possibly be transported either horizontally or vertically from a remote production zone to the measurement site. Before scrutinizing this aspect in more detail, we need to know about the time required for freshly produced particles to reach detectable sizes > 3 nm. Assuming a linear diameter growth which time and using the average growth rate of 2.6 nm h^{-1} (cf. Sect. 6.1), the observed nucleation mode particles would be at least about 1 hour old. Horizontal transport can be ruled out since it appears to be extremely improbably to assume a production zone in either direction from the observation site at 1 h distance. Notably, the closed distributions were observed in air masses from all directions, and the mesoscale extension of the NPF events suggests spatially uniform atmospheric conditions. Vertical transport from a localised source region could principally imply two possible production zones: one at the top of the boundary layer (cf. Sect. 5.3, and also the discussion in the companion paper, Uhrner et al., 2002) where the thermodynamic conditions are more favourable for nucleation, and one near the ground, where the sources of substantial biogenic precursor emissions are. The agreement found between the particle size distributions at the MOHP mountain site (above forested area) and a low-level site (within the forest) (cf. Fig. 2) gave, however, no indication for a particle formation within the immediate surface layer. Furthermore,

the seasonal distribution of NPF events with its highest frequency observed in winter and spring (cf. Fig. 6) can only be explained if precursors different from biogenic vapours (such as H_2SO_4) are in control of nucleation. The alternative scenario, assuming production near the top of the boundary is not free of complications either: Convective mixing communicates concentration changes within the boundary layer on a time scale of typically 15 min; this is, however, substantially shorter than the time lag of at least 1 h required for particle growth. In this scenario, newly formed particles would lack the time to grow to the observed sizes if their observed growth rates were valid for sizes smaller than 3 nm. In addition, the MOHp measurement site was often near or slightly above the inversion layer during NPF events observed in the cold season. It appears thus improbable that particle nucleation never occurred in the same air layer as the measurement site. Despite this, the observed size distributions were always closed. As an exit to the problem, one could think of a nonlinear growth of the nucleation mode particles with time, possibly caused by higher precursor concentrations at the top of the boundary layer. Such a hypothesis could only be verified by a vertically resolved modeling simulations.

The second hypothesis would require a growth mechanism that causes nucleation mode particles of different sizes to grow at different rates. Newly formed particles can only merge into a stable and growing nucleation mode if they survive passage through the size range 1–10 nm without coagulating (e.g. Kerminen et al., 2001). Since the life-times of particles against coagulation are increasingly shorter with decreasing particle size, and the size distributions decrease monotonically below ca. 6 nm, this hypothesis requires an increasing particle growth rate with decreasing diameters. We do not know which mechanism could fulfil this behaviour. One could speculate about a contribution by ion-mediated growth which principally favors growth of the smallest particles (Yu and Turco, 2000) but a quantitative test with a complex model of the particle dynamics is out of the scope of this paper.

8 Conclusions

Atmospheric new particle formation (NPF) events were detected and classified over a period of 2.5 years of observations. NPF events occurred on 18% of all measurement days, typically during midday hours under relatively sunny and low humidity conditions. The typical horizontal dimension of the air masses in which NPF events occur was estimated to be ~100 km or larger, while concurrent measurements at two different altitudes suggested a very homogeneous distribution of newly formed particles within several kilometres around the observation point. The concentrations of newly formed particles correlated significantly with solar irradiance and ambient levels of H_2SO_4. Especially in the cold season, an anti-correlation was observed with humidity and the con-

densational sink related to the pre-existing particle surface area. The latter favourable conditions were mainly caused by warm, dry, and relatively clean air masses from southerly directions subsiding north of the Alpine mountain chain.

Experimentally determined particle formation rates during NPF events were calculated to be on average 1 $cm^{-3} s^{-1}$, with the range: 0.01–9 $cm^{-3} s^{-1}$. The calculated ternary homogeneous H_2SO_4-NH_3-H_2O nucleation rates, based on measured $[H_2SO_4]$ and $[NH_3]$=100 pptV, were wider scattered but in agreement with the experimental formation rates within a few orders of magnitude. Assuming a vertical cycling of air within the mixed layer, the picture of the comparison improved: The thermodynamic conditions near the mixed layer top were found to potentially enhance the ternary nucleation rate by six orders of magnitude. This ternary rate was for 95% of the NPF events in agreement with the experimentally determined particle formation rate within a factor range of 10^{-2}–10^4. Meanwhile, no indications were found that reaction products of organic compounds would directly control the occurrence of NPF events.

The growth rates of nucleation mode particles showed a seasonal cycle with higher growth rates up to 9 $nm h^{-1}$ in the summer and below 3 $nm h^{-1}$ in the months October to February. Particle formation intensity and nucleation mode particle growth appeared not to be correlated. A fraction of the particle growth rates was explained by the co-condensation of H_2SO_4-H_2O-NH_3. In some cases this was close to 100% but mostly it accounted for 50% or less of the observed growth rates. The "missing growth rate" could potentially be provided by condensable organic vapours: based on calculated atmospheric turn-over rates due to OH and O_3 it is expected that the oxidation products of monoterpenes contribute to the observed particle growth, particularly in the warm season. However, no clear correlation between the terpene turn-over rate and the missing particle growth rate was identified, which might be a consequence of the restricted data available and the simplistic assumption that turn-over is a measure for condensational growth due to organics.

In spite of all new findings, an exact determination of the factors that ultimately control the occurrence of NPF events at Hohenpeissenberg proved to be difficult. Although several correlations and anti-correlations, respectively, were established between the particle formation intensity, solar radiation, sulfuric acid, the condensational sink CS, and meteorological factors, no global set of threshold criteria could be defined to effectively separate event days and non-event days. On a large number of non-event days, ternary nucleation theory predicts numbers of new nano-particles easily comparable to those on event days. It may turn out that understanding the occurence of NPF events is linked to the question, why the particle size distributions were closed at the smallest diameters. This points either towards NPF at the top of the boundary layer, or a non-linear particle growth rate below 3 nm. Answering these questions will require more intensive studies including vertical profiles of particle size

distributions and precursor gases, as well as developements of aerosol measurement techniques down to the size range of nucleation (1 nm). Such studies could then provide the neccessary information to test NPF mechanisms in detailed model simulations.

References

Berresheim, H., Elste, T., Plass-Dülmer, C., Eisele, F. L., and Tanner, D. J.: Chemical ionization mass spectrometer for long-term measurements of atmospheric OH and H_2SO_4, Int. J. Mass Spectrom., 210–211, 2000.

Birmili, W. and Wiedensohler, A.: New particle formation in the continental boundary layer: Meteorological and gas phase parameter influence, Geophys. Res. Lett., 27, 3325–3328, 2000.

Birmili, W., Stratmann, F., Wiedensohler, A., Covert, D., Russell, L. M., and Berg, O.: Determination of differential mobility analyzer transfer functions using identical instruments in series, Aerosol Sci. Technol., 27, 215–223, 1997.

Birmili, W., Stratmann, F., and Wiedensohler, A.: Design of a DMA-based size spectrometer for a large particle size range and stable operation, J. Aerosol Sci., 30, 549–553, 1999.

Birmili, W., Wiedensohler, A., Plass-Dülmer, C., and Berresheim, H.: Evolution of newly formed aerosol particles in the continental boundary layer: A case study including OH and H_2SO_4 measurements, Geophys. Res. Lett., 27, 2205–2209, 2000.

Clarke, T. D.: Atmospheric nuclei in the Pacific midtroposphere: Their nature, concentration and evolution, J. Geophys. Res., 98D, 20 633–20 647, 1993.

Clement, C. F., Pirjola, L., dal Maso, M., Mäkelä, J. M., and Kulmala, M.: Analysis of particle formation bursts observed in Finland, J. Aerosol Sci., 32, 217–236, 2001.

Coe, H., Williams, P., McFiggans, G., Gallagher, M., Beswick, K., Bower, K., and Choularton, T.: Behavior of ultrafine particles in continental and marine air masses at a rural site in the united kingdom, J. Geophys. Res., 105, 26 891–26 905, 2000.

Coffman, D. J. and Hegg, D. A.: A preliminary study of the effect of ammonia on particle nucleation in the marine boundary layer, J. Geophys. Res., 100, 7147–7160, 1995.

Covert, D. S., Kapustin, V. N., Quinn, P. K., and Bates, T. S.: New particle formation in the marine boundary layer, J. Geophys. Res., 97, 20 581–20 589, 1992.

Easter, R. C. and Peters, L. K.: Binary homogeneous nucleation: Temperature and relative humidity fluctuations, nonlinearity, and aspects of new particle formaton in the atmosphere, J. Appl. Met., 33, 775–784, 1994.

Friedlander, S. K.: Smoke, Dust, and Haze, Oxford University Press, New York, 2000.

Georgelin, M. R., El-Khatib, R., and Lemaire, Y.: Why is a model topography still not described accurately enough at mesoscale?

What we have learned from the compare experiment?, in Workshop on Orography, pp. 199–227, ECMWF, Bracknell, 1997.

Guenther, A. B., Zimmerman, P. R., Harley, P. C., Monson, R. K., and Fall, R.: Isoprene and monoterpene emission rate variability: model evaluations and sensitivity analyses, J. Geophys. Res., 98, 12 609–12 617, 1993.

Haywood, J. and Boucher, O.: Estimates of the direct and indirect radiative forcing due to tropospheric aerosols: A review, Rev. Geophys., 38, 513–543, 2000.

Hoffmann, T., Odum, J. R., Bowman, F., Collins, D., Klockow, D., Flagan, R. C., and Seinfeld, J. H.: Formation of organic aerosols from the oxidation of biogenic hydrocarbons, J. Atmos. Chem., 26, 189–222, 1997.

Holzworth, C. G.: Estimates of mean maximum mixing depths in the contiguous United States, Mon. Wea. Rev., 92, 235–242, 1964.

Hõrrak, U., Salm, J., and Tammet, H.: Bursts of intermediate ions in atmospheric air, J. Geophys. Res., 103, 13 909–13 915, 1998.

Hõrrak, U., Salm, J., and Tammet, H.: Statistical characterisation of air ion mobility spectra at tahkuse observatory: Classification of air ions, J. Geophys. Res., 105, 9291–9302, 2000.

Houghton, J., Ding, Y., Griggs, D., Noguer, M., van der Linden, P., and Xiaosu, D. (Eds): Climate Change 2001: The Scientific Basis, IPCC, Cambridge Univ. Press, contribution of Working Group I to the Third Assessment Report of the Intergovernmental Panel on Climate Change (IPCC), 2001.

Karg, E., Ferron, G. A., Busch, B., and Heyder, J.: Growth behaviour and aqueous fraction of atmoshperic particles in dependence of relative humidity (in German), Final report BII7 Bay-FORKLIM, GSF, Neuherberg, Germany, 1999.

Kavouras, I., Mihalopoulos, N., and Stephanou, E. G.: Secondary aerosol formation vs. primary organic aerosol emission: In situ evidence for the chemical coupling between monoterpene acidic photo-oxidation products and new particle formation over forests, Env. Sci. Technol., 33, 1028–1037, 1999.

Kerminen, V.-M., Pirjola, L., and Kulmala, M.: How significantly does coagulational scavenging limit atmospheric particle production?, J. Geophys. Res., 125, 24 110–24 125, 2001.

Kulmala, M., Pirjola, L., and Mäkelä, J. M.: Stable sulphate clusters as a source of new atmospheric particles, Nature, 404, 66–69, 2000.

Mäkelä, J. M., Aalto, P., Jokinen, V., Pohja, T., Nissinen, A., Palmroth, S., Markkanen, T., Seitsonen, K., Lihavainen, H., and Kulmala, M.: Observation of ultrafine aerosol particle formation and growth in boreal forest, Geophys. Res. Letters, 24, 1219–1222, 1997.

Mäkelä, J. M., Dal Maso, M., Pirjola, L., Keronen, P., Laakso, L., Kulmala, M., and Laaksonen, A.: Characteristics of the aerosol particle formation events observed at a boreal forest site in southern Finland, Boreal Env. Res., 5, 299–313, 2000.

McMurry, P. H., Woo, K. S., Weber, R., Chen, D.-R., and Pui, D. Y. H.: Size distributions of 3 to 10 nm atmospheric particles: Implications for nucleation mechanisms, Phil. Trans. Royal Soc., A358, 2625–2642, 2000.

Napari, I., Noppel, M., Vehkamäki, H., and Kulmala, M.: Parametrization of ternary nucleation rates for H_2SO_4-NH_3-H_2O vapors., J. Geophys. Res., 107, manuscript No. 2002JD002132, in press., 2002a.

Napari, I., Noppel, M., Vehkamäki, H., and Kulmala, M.: An im-

proved model for ternary nucleation of sulphuric acid-ammonia-water., J. Chem. Phys., 116, 4221–4227, 2002b.

Nilsson, E. D. and Kulmala, M.: The potential for atmospheric mixing processes to enhance the binary nucleation rate, J. Geophys. Res., 103, 1381–1389, 1998.

Nilsson, E. D., Pirjola, L., and Kulmala, M.: The effect of atmospheric waves on aerosol nucleation and size distribution, J. Geophys. Res., 105, 19 917–19 926, 2000.

Nilsson, E. D., Paatero, J., and Boy, M.: Effects of air masses and synoptic weather on aerosol formation in the continental boundary layer, Tellus, 53B, 462–478, 2001a.

Nilsson, E. D., Rannik, U., Kulmala, M., Buzorius, G., and O'Dowd, C. D.: Effects of continental boundary layer evolution, convection, turbulence, and entrainment on aerosol formation, Tellus, 53B, 441–461, 2001b.

O'Dowd, C., Jimenez, J., Bahreini, R., Flagan, R., Seinfeld, J., Hämeri, K., Pirjola, L., Kulmala, M., Jennings, S., and Hoffmann, T.: Marine aerosol formation from biogenic iodine emissions, Nature, 417, 632–636, 2002a.

O'Dowd, C. D., Hämeri, K., Aalto, P., and Kulmala, M.: First experimental evidence of new particle formation from organic vapours over forests, Nature, 416, 497–498, 2002b.

Raes, F.: Entrainment of free tropospheric aerosols as a regulating mechanism for cloud condensation nuclei in the remote boundary layer, J. Geophys. Res., 100, 2893–2903, 1995.

Ravishankara, A. R.: Heterogeneous and multiphase chemistry in the troposphere, Science, 276, 1058–1065, 1997.

Reischl, G. P., Mäkelä, J. M., and Necid, J.: Performance of a Vienna type differential mobility analyzer at 1.2–20 nanometer, Aerosol Sci. Technol., 27, 651–672, 1997.

Seinfeld, J. H. and Pandis, S. P.: Atmospheric Chemistry and Physics, John Wiley, New York, 2 edn., 1998.

Spindler, G., Teichmann, U., and Sutton, M. A.: Ammonia dry deposition over grassland-micrometeorological flux-gradient measurements and bidirectional flux calculations using an inferential model, Q. J. Royal Met. Soc., 127, 795–814, 2001.

Swietlicki, E., Zhou, J., Berg, O. H., Martinsson, M. G., Frank, G., Cederfelt, S. I., Dusek, U., Berner, A., Birmili, W., Wiedensohler, A., Yuskiewicz, B., and Bower, K. N.: A closure study of sub-micrometer aerosol particle hygroscopic behaviour, Atmos. Res., 50, 205–240, 1999.

Uhrner, U., Birmili, W., Stratmann, F., Wilck, M., Ackermann, I. J., and Berresheim, H.: Particle formation at a continental background site: comparison of model results with observations, Atmos. Chem. Phys. Discuss., 2, 2413–2448, 2002.

Weber, R. J., Marti, J. J., McMurry, P. H., Eisele, F. L., Tanner, D. J., and Jefferson, A.: Measurement of new particle formation and ultrafine particle growth rates at a clean continental site, J. Geophys. Res., 102, 4375–4385, 1997.

Weber, R. J., McMurry, P. H., III, R. L. M., Tanner, D. J., Eisele, F. L., Clarke, A. D., and Kapustin, V. N.: New particle formation in the remote troposphere: A comparison of observations at various sites, Geophys. Res. Lett., 26, 307–310, 1999.

Wiedensohler, A.: An approximation of the bipolar charge distribution for particles in the submicron range, J. Aerosol Sci., 19, 387–389, 1988.

Wiedensohler, A., Covert, D. S., Swietlicki, E., Aalto, P., Heintzenberg, J., and Leck, C.: Occurrence of an ultrafine particle mode less than 20 nm in diameter in the marine boundary layer during Arctic summer and autumn, Tellus, 48B, 213–222, 1996.

Winklmayr, W., Reischl, G. P., Linde, A. O., and Berner, A.: A new electromobility spectrometer for the measurement of aerosol size distributions in the size range from 1 to 1000 nm, J. Aerosol Sci., 22, 289–296, 1991.

WMO2003: Global Atmosphere Watch (GAW), World Meteorological Organization, http://www.wmo.ch/web/arep/gaw_home.html, 2003.

Yu, F. and Turco, R. P.: Ultrafine aerosol formation via ion-mediated nucleation, Geophys. Res. Lett., 27, 883–886, 2000.